

High Harmonic Generation by Guided Surface Plasmon Polaritons

Joonhee Choi, Seungchul Kim, In-Yong Park, Seung-Woo Kim*

Ultrafast Optics for Ultraprecision Group, Korea Advanced Institute of Science and Technology (KAIST), Science Town, Daejeon, 305-701, South Korea

ABSTRACT

We discuss how the intriguing phenomenon of surface plasmon resonance (SPR) can be exploited in enhancing the intensity field of the incident femtosecond laser for the purpose of high harmonic generation (HHG). We first summarize our previous attempt made with a 2-D planar nanostructure comprised of metallic bow-tie nano-antennas, which enabled us to generate up to 21st harmonics from Xenon gas using 1-nJ pulse energy with an intensity enhancement factor of ~20 dB. Then we describe another attempt currently being made by devising a 3-D nano-waveguide with the aim of improving the HHG conversion efficiency by expanding the localized volume of field enhancement by means of propagating surface plasmon polaritons (SPPs). Our finite-difference time-domain (FDTD) calculation shows that the enhanced volume can be increased significantly by optimal selection of the waveguide's geometrical parameters as verified in our preliminary experimental results.

Keywords: surface plasmon resonance, surface plasmon polaritons, high harmonic generation, 3-D waveguide, finite-difference time-domain analysis, extreme ultraviolet radiation.

1. INTRODUCTION

Surface plasmon polaritons (SPPs) are surface electromagnetic waves that propagate in a direction parallel to the metal/dielectric interface as a result of collective electronic resonance occurring in response to the incident light [1]. The evanescent nature of SPPs is very sensitive to any change of the boundary, such as the absorption of molecules to the metal surface, permitting investigating atoms or molecules with enhanced sensitivity at sub-wavelength spatial resolution. Examples include surface enhanced Raman spectroscopy [2], molecular sensing [3,4] and near-field scanning optical microscopy [5]. The transmission behavior of SPPs through various forms of waveguides is also studied in designing photonic circuits with much smaller device sizes compared to their counter parts of electronic circuits [6].

Another intriguing feature of SPPs is associated with locally enhanced near field as observed in a tapered waveguide [7] or dipole nano-antenna [8,9]. When SPPs are guided to a narrow region, the field enhancement factor defined as the ratio of the enhanced field to the incident field could readily reach 20-30 dB in terms of intensity. This allows one to attain huge peak intensities needed for various nonlinear optical phenomena from a moderate-power laser pulse without actual power amplification.

High harmonic generation (HHG) is a well-known interaction of light with bound electrons, which produces coherent short radiation in the extreme-ultraviolet (EUV), or even soft X-ray range [10]. Triggering the HHG process requires a strong laser field whose intensity level exceeds 10^{13} Wcm⁻² [11]. Such a high intensity field is not attainable simply from a single femtosecond laser oscillator, thus chirped-pulse amplification (CPA) [12] or intra-cavity amplification [13] is widely adopted to boost the pulse intensity. Although both the extra-cavity techniques enable one to obtain high intensities for HHG, they are subject to some technical restrictions. CPA involves not only additional pumping power but also reduction of the pulse repetition rate of the original oscillator to protect the amplifying crystal or fiber from thermal damage. Besides, the intra-cavity technique works properly only when the group delay dispersion (GDD) caused by the intra-cavity is well compensated for through elaborate cavity control.

Enhancing the pulse intensity by means of localized SPPs requires neither pulse rate reduction nor GDD compensation. By inducing surface plasmon waves in a resonant mode to the incident femtosecond laser using well-designed plasmonic nanodevices, high laser fields exceeding the threshold intensity for HHG can be readily generated without complex amplification schemes relying on extra cavities.

*swk@kaist.ac.kr; phone: +82-42-350-3217; fax: +82-42-350-3210

Our previous work demonstrated a HHG scheme of using a bow-tie nano-antenna array made of Au on a sapphire substrate. This 2-D planar nanostructure enabled us to generate up to 21st harmonics from Xenon gas using 1-nJ pulse energy with an intensity enhancement factor of ~ 20 dB [14]. The HHG conversion efficiency was in the range of 10^{-9} to 10^{-10} when the input pulse intensity was $\sim 10^{11}$ W/cm². The relatively low conversion efficiency was attributable to the small volume of field enhancement that is narrowly confined to the 20-nm gap between a pair of triangular patches constituting a bow-tie, which limits the interaction length with gases in which the HHG process actually takes place. Furthermore, the input pulse intensity could not be raised further due to the thermal damage on the nano-antenna array of 50 nm thickness.

In this paper, with the aim of improving the HHG efficiency, we introduce another type of nanostructure that offers a large volume of field enhancement by guiding SPPs more efficiently [15]. The waveguide resembles a tapered hollow funnel with metal cladding having a negative dielectric constant along with a relatively small imaginary part such as gold and silver [16]. When a femtosecond laser enters into an optimally-shaped tapered waveguide, the laser field is converted into propagating SPPs and guided toward the inner side of the tapered waveguide with deceleration. In consequence, SPPs are accumulated near the exit aperture of the waveguide whose dimension is in the sub-wavelength scale. This results in a substantial increase in the intensity enhancement of the incident laser field. By FDTD (Finite-Difference Time-Domain) simulation, we calculate the field-enhanced volume as well as the intensity enhancement factor with subsequent optical selection of the design parameters of the suggested tapered waveguide. The plasmonic waveguide structure is finally fabricated on the tip of a modified NSOM probe so that this new compact type of coherent EUV light source can efficiently be incorporated with various applications of near-field optics such as Raman spectroscopy [17], microscopy [18] and lithography [19].

2. PLASMONIC NANODEVICE DESIGN

2.1 2-D nano-antenna structures for localized surface plasmon resonance

A single nano-object can enhance the incident laser intensity around its surface by locally induced SPPs, which is simply called the lightning-rod effect [20]. Two nano-objects placed close to each other can constitute a nanostructure that gives stronger field enhancement over a wider volume than a single nano-object [21]. Among various nanostructure configurations, the rectangular dipole antenna structure as well as the triangular-shaped bow-tie structure draws attention due to their simple geometries from the viewpoint of fabrication [22]. The overall shape and necessary parameters for each plasmonic nanoantenna structure are shown in the fig. 1.

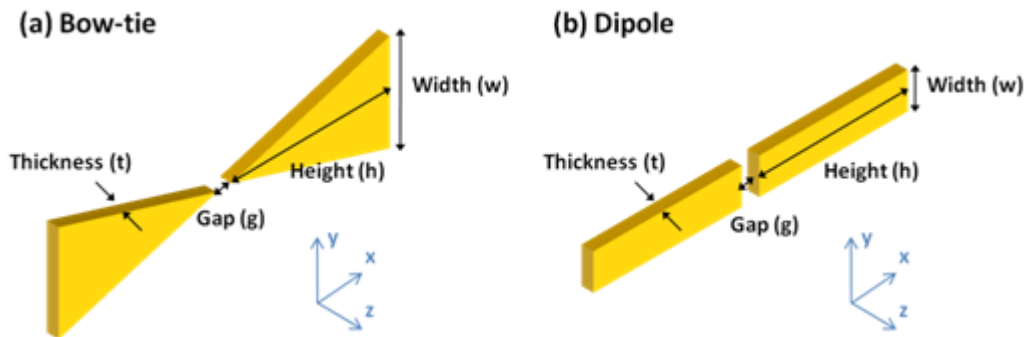


Fig. 1 Two planar nanostructures considered for local surface plasmon resonance and their design parameters: (a) Bow-tie and (b) Dipole rods.

As shown in Fig. 1, there are four design parameters determining the overall geometry of each nanostructure; the width (w), height (h), gap (g) and thickness (t). For efficient high harmonic generation (HHG), the geometry has to be designed to provide not only a higher field enhancement factor but also a large field-enhanced volume. In this context, we carried out design optimization of the nanostructures by calculating the resulting enhanced field using finite-difference time-

domain (FDTD) simulation for various combinations of the four design parameters. For the purpose, we counted on a commercial software package of electrodynamics analysis named XFDTD[®]6.3 (REMCOM), which enables us to directly solve the Maxwell equations as the incident femtosecond pulse proceeds to the nanostructure with a given set of boundary conditions. Fig. 2 shows several snapshot images when surface plasmon resonance takes place for in each nanostructure. After many trials, the design parameters of nanostructures are selected as follows: for the bow-tie, $w = 90$ nm, $h = 175$ nm, $g = 20$ nm and $t = 50$ nm, while for the dipole rod $w = 50$ nm, $h = 175$ nm, $g = 20$ nm, and $t = 70$ nm. The incident laser field is assumed linearly polarized in the x-direction along the antenna axis, with a center wavelength of 800 nm and pulse width of 10 fs (FWHM).

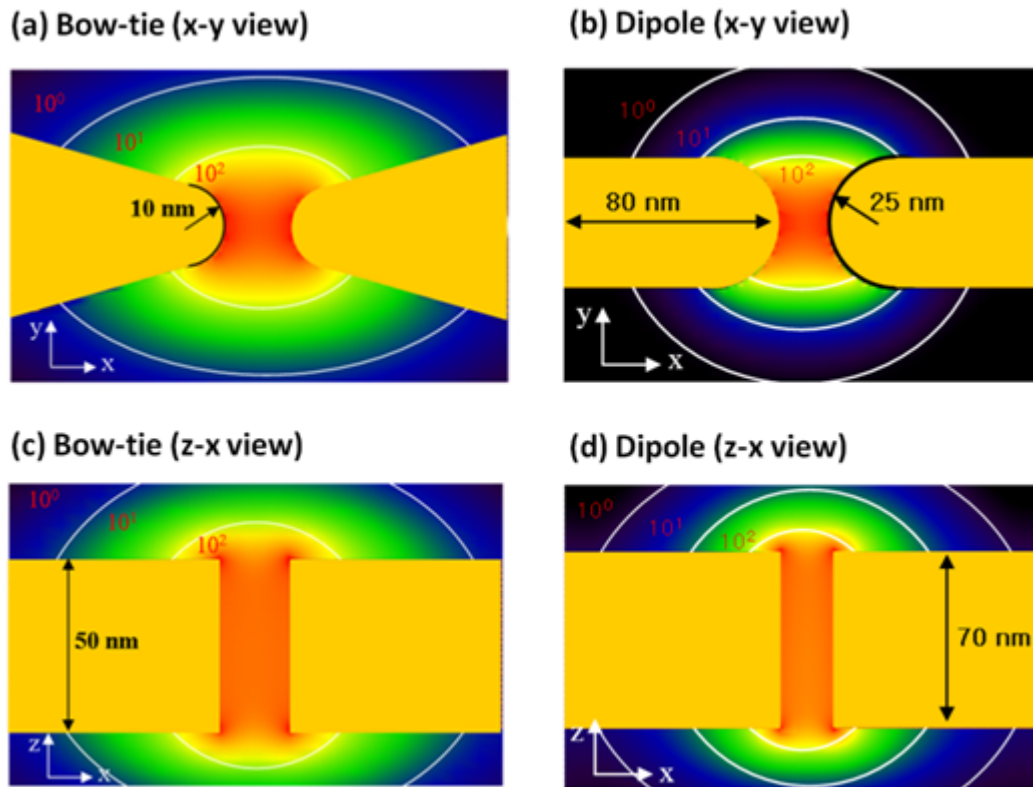


Fig. 2 Contour lines of enhanced intensity field obtained by FDTD calculation of local surface plasmon resonance for bow-tie and dipole rod nanostructures. Optimized dimensions are: for the bow-tie, $w = 90$ nm, $h = 175$ nm, $g = 20$ nm and $t = 50$ nm, while for the dipole rod, $w = 50$ nm, $h = 175$ nm, $g = 20$ nm and $t = 70$ nm. (a) the enhanced field seen on the x-y plane of the bow-tie nanostructure, (b) Enhanced field on the x-y plane of the dipole rod nanostructure, (c) The z-x plane view of the bow-tie nanostructure, (d) the z-x plane view of the dipole nanostructure. Note that the tips are assumed to have rounded edges to reflect imperfect fabrication in calculation.

The computational result shown in Fig. 2 reveals that the enhanced field always maintains a symmetrical distribution, which becomes large along the edges and also in the gap in the middle. The intensity enhancement factor exceeds 20 dB at its maximum in both the cases of bow-tie and dipole rod, which is sufficient to attain intensities stronger than the HHG triggering threshold of 10^{13} W/cm² from a moderate femtosecond laser oscillator emitting a few nJ pulse power with a pulse width of 10 fs. This low pulse energy can lead to a maximum intensity of 10^{11} W/cm² at most when a well-aligned high-NA focusing lens is appropriately incorporated. The spatial volume in which the induced intensity exceeds 20 dB turns out to be larger in the case of bow-tie, which yields a volumetric size of 30 nm x 40 nm x 50 nm. To increase the overall HHG conversion efficiency, multiple bow-ties are arranged in a 2-D array so that as many as about fifty bow-ties are densely populated within the focal area of the incident laser. The bow-ties and dipole rods are fabricated by either the FIB (focused ion beam) process or the E-beam lithography technique. The FIB process is advantageous in achieving high

geometrical accuracy in fabricated patterns, while the E-beam litho process offers a shorter fabrication time particularly when a large array pattern needs to be made with many nanostructures.

Our experiment using bow-ties verifies that the shortest EUV wavelength generated by HHG lies in the cut-off spectral region of 30 ~ 40 nm, which confirms that the intensity enhancement factor actually realized reaches at least a factor of 300. This nanostructure based HHG consequently demonstrates a practical possibility of developing a compact table-top sized coherent EUV laser source [23].

2.2 3-D tapered waveguide accumulating surface plasmon polaritons

Although the aforementioned planar nano-antenna structures are basically capable of performing HHG, they have two common weak points to be improved: First, the achievable HHG conversion efficiency is low in the range of 10^{-9} to 10^{-10} . Second, the lifetime is short due to the thermal deformation or damage caused by the focused high power laser source as the maximum enhancement occurs at the metal-air interface surface.

It is well-known that an incident laser field can amplify itself while propagating along the surface of tapered geometry as demonstrated in a DMD (dielectric-metal-dielectric) tapered waveguide [24] and a MDM (metal-dielectric-metal) tapered waveguide [25]. The DMD tapered waveguide is in fact a 2-D metallic tip that has a very short tip-radius at its end. The resulting intensity field is enhanced by a factor of more than 10^4 near the sharp edge of the tip, which in turn largely improves the near-field monitoring sensitivity. On the other hands, the MDM tapered waveguide is capable of increasing the peak intensity of the fundamental light and also it can emit the visible light through the sub-wavelength aperture. For these reasons, the MDM tapered waveguide can act as an aperture-type NSOM probe.

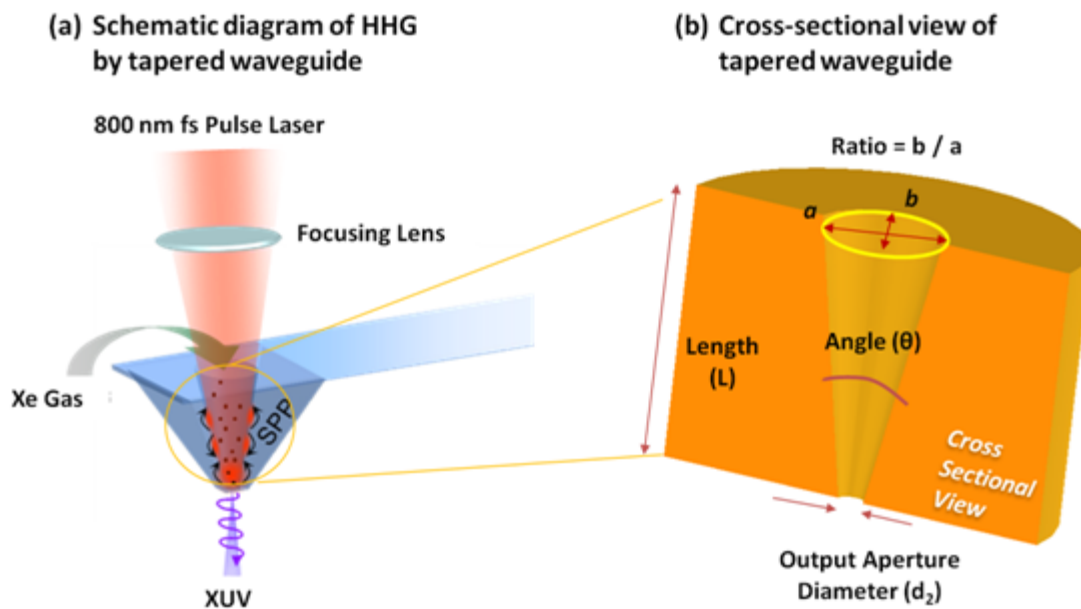


Fig. 3 (a) Conceptual diagram of HHG by the MDM tapered conical waveguide and (b) the simulation parameters for the tapered waveguide. Note that the aperture has a shape of ellipse and the waveguide is attached onto a cantilever to be used for near-field application. The waveguide material is silver which has low loss in the visible and near-infrared light.

In principle, the field enhancement in the tapered geometry arises from the gradual accumulation of SPPs energy as excited SPPs propagate towards the sub-wavelength-scale region of the waveguide. In the MDM tapered waveguide whose cross-section takes either a circular or elliptical shape, the guided fundamental mode maintains a Gaussian distribution; the highest intensity exists through the central core axis of the waveguide [26]. Hence, EUV light can be generated without critical thermal degradation in the 3-D MDM tapered waveguide, which is never possible with 2-D bowtie nano-antennas. In addition, various forms of near-field optical investigations in the EUV region could be easily

performed provided that the designed MDM tapered waveguide is fabricated in a similar way to the aperture-type NSOM probe.

According to these basic advantages of the MDM tapered waveguide, we attempt to replace our previous planar nanoantennas with a MDM tapered conical waveguide structure. Fig. 3 describes the conceptual shape and design parameters of the tapered conical waveguide. The waveguide material is assumed as silver in simulation, which has the lowest loss in the visible and the near-infrared range among many candidate metals. Also, the core dielectric region is made to have an elliptical cross-section. As in the case of 2-D nanoantenna structures, similar FDTD optimization analysis was performed with four design parameters being the waveguide length (L), output aperture diameter (d_2), angle (θ) and the ratio of the minor axis to the major axis (b/a) of the dielectric cross-section. Both the output aperture diameter and the axis ratio are measured on the plane containing the major axis of the ellipse. Fig. 4 shows the simulation result that explains how the field enhancement factor depends on the design parameters. The 20-dB volume represents the spatial volume in which the intensity is enhanced more than 20 dB.

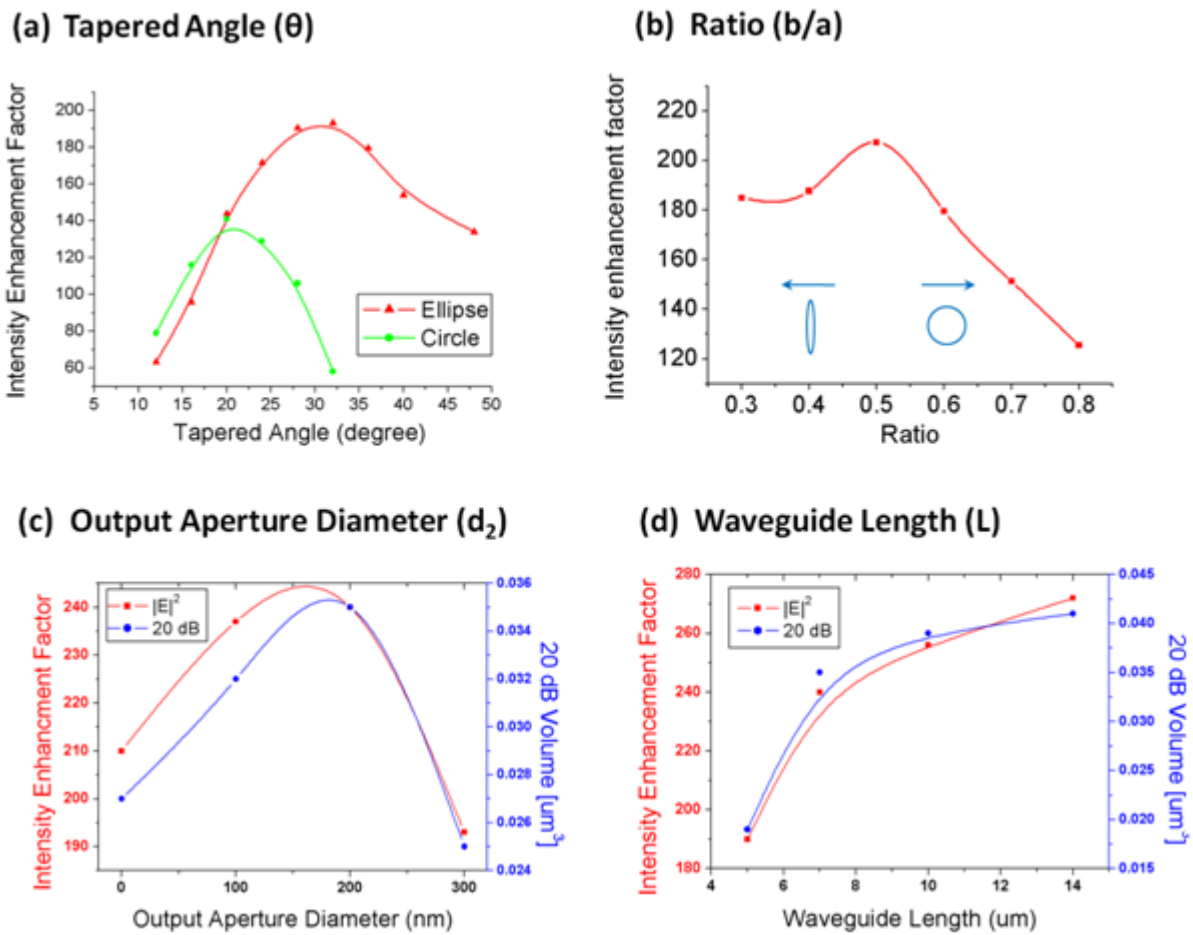


Fig. 4 FDTD simulation results showing how the maximum intensity enhancement factor as well as the 20-dB volume depend on the waveguide parameters; (a) tapered angle, (b) axis ratio, (c) output aperture diameter and (d) waveguide length; In Fig. 4(a), the elliptical waveguide is defined as $b/a = 0.5$, $d_2 = 200$ nm and $L = 5$ μm . Note that $b/a = 1$ for the circular waveguide. In Fig. 4(b), $\theta = 28^\circ$, $L = 6$ μm , and $d_2 = 200$ nm. In Fig. 4(c), $b/a = 0.5$, $\theta = 28^\circ$ and $L = 7$ μm . In Fig. 4(d), $b/a = 0.5$, $\theta = 28^\circ$ and $d_2 = 200$ nm.

Fig. 4(a) indicates that there is an optimal value for the taper angle. This is due to the fact that propagating SPPs along the tapered inner surface are subject to much SPP coupling loss if the taper angle is too small. On the other hand, the reflection loss becomes dominant when the taper angle is too large. The SPP coupling loss is caused by ineffective phase-matching between the incident photon and the excited surface plasmon. The reflection loss results from insufficient accumulation of SPPs near the output aperture. Therefore, there should be a trade-off between the SPP coupling loss and reflection loss, which eventually leads to an optimal taper angle for each waveguide of different cross-section. In general, the elliptical waveguide yields a larger intensity enhancement factor than the circular waveguide provided that the polarization direction of the incident laser is parallel to the minor axis of the elliptical cross-section. When the axis ratio 0.5, the intensity enhancement factor reaches its maximum of about 200. Repeated computation with varying taper angles and axis ratios concludes that $\theta = 28^\circ$ and $b/a = 0.5$ are the optimum combination giving the highest field enhancement.

Fig. 4(c) and Fig. 4(d) depict the dependence of the field enhancement factor and 20-dB volume upon the output aperture diameter and waveguide length, respectively. Fig. 4(c) also shows there also exists the optimal aperture size that yields both the highest peak intensity enhancement factor and the largest 20-dB volume. This is due to the balance between the back reflection loss and the radiation leakage loss of SPPs. If the output aperture diameter is too small, the portion of back reflected SPPs increases so that they attenuate the field enhancement factor. On the other hand, if the output diameter size increases up to the half wavelength scale, the radiation leakage becomes dominant. Therefore, selecting a proper output diameter size is important in order to accumulate the energy of SPPs with decreasing group velocity as much as possible near the end of the waveguide. In Fig. 4(d), both the maximum intensity enhancement factor and the 20 dB volume gradually increase with increasing the waveguide length. However, the two values become saturated when the waveguide length is larger than $\sim 10 \mu\text{m}$.

In consideration of the above trend analysis, the optimal design parameters for the MDM tapered elliptical waveguide are determined. Chosen values are $\theta = 28^\circ$ (14°), $d_2 = 200 \text{ nm}$ (100 nm) along the major (minor) axis direction, $L = 9 \mu\text{m}$, and $b/a = 0.5$. Fig. 5 shows the calculated near field distribution of the tapered waveguide through FDTD simulation. Dimensions of the 20-dB volume are calculated as $400 \text{ nm} \times 300 \text{ nm} \times 300 \text{ nm}$ in the x , y and z direction, respectively. Although the peak field enhancement factor is smaller than that of 2-D nanoantenna devices which depends on local LSP resonance, the size of the 20-dB volume is worked out roughly three orders of magnitude larger than that of a single bow-tie nanoantenna pair. Also, the location where the maximum field enhancement occurs is not at the metallic surface but at the core region which is in vacuum. This feature implies that the 3-D MDM waveguide structure has an inherent potential of being more thermally robust than 2-D nanoantenna structures.

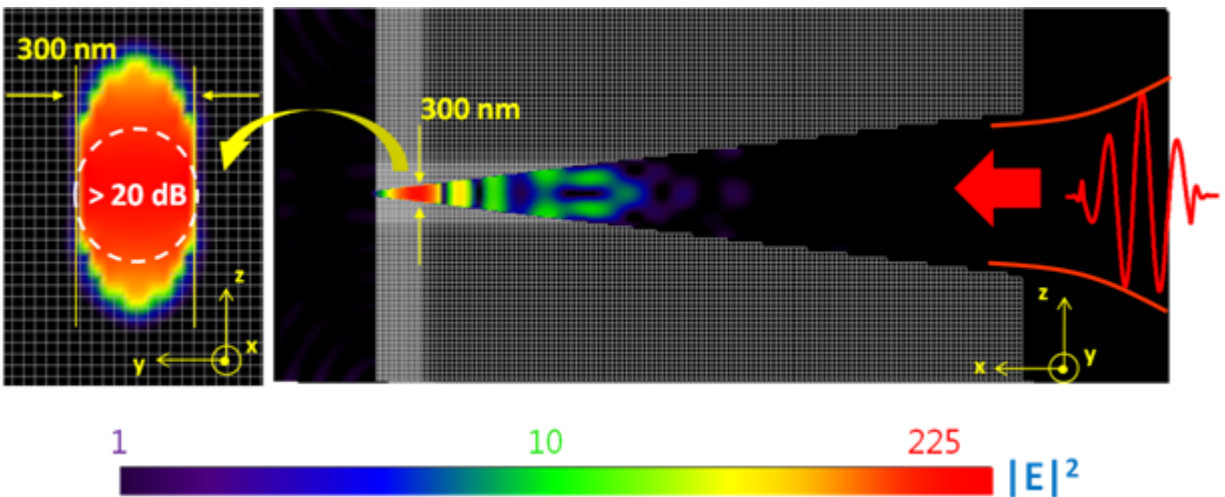


Fig. 5 Intensity enhancement and distribution images of FDTD simulation when maximal field enhancement is obtained by accumulation of propagating SPPs. Left inset shows the cross-sectional view of the optimized tapered waveguide

whose dimensions are $\theta = 28^\circ$, $d_2 = 200$, $b/a = 0.5$ and $L = 9 \mu\text{m}$. The inlet elliptical aperture size where the incident laser field enters is $4 \mu\text{m} \times 2 \mu\text{m}$ in the major and minor axis direction, respectively.

3. FABRICATION OF 3-D PLASMONIC WAVEGUIDE STRUCTURE

The 3-D MDM tapered plasmonic waveguide was fabricated using the FIB technique while the actual fabrication process was monitored real time. As a first step, a 10- μm thick silver film was deposited onto a substrate that is a commercial cantilever-based NSOM probe having a hollow pyramidal gap located at the end of its thin and long cantilever [27].

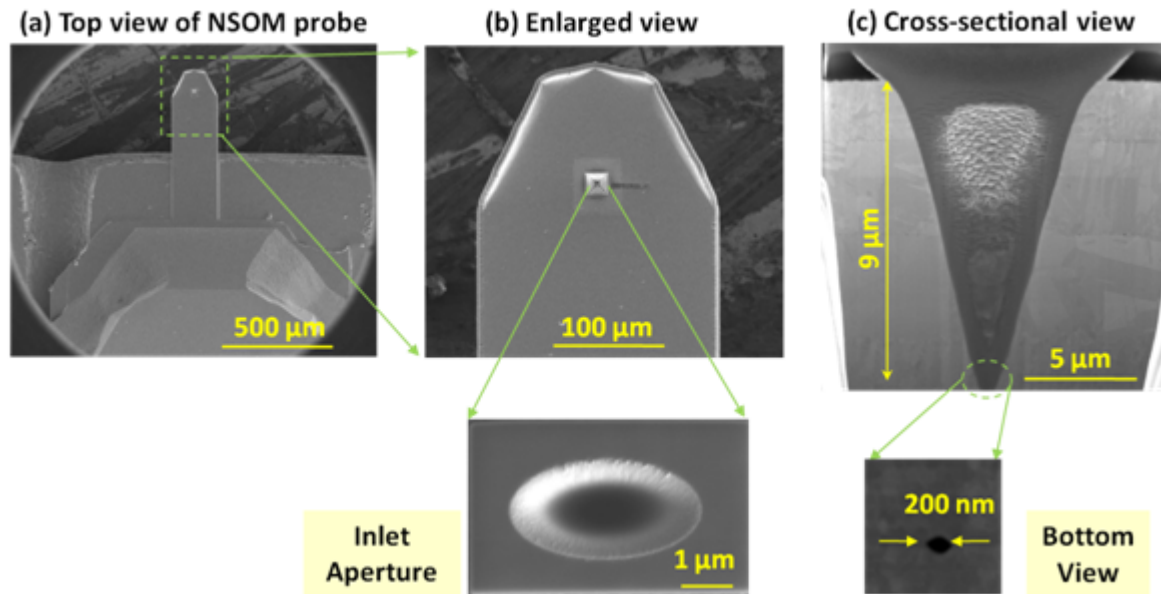


Fig. 6 SEM images of the fabricated tapered waveguide structure embedded in a NSOM probe tip, (a) top view of the NSOM probe, (b) Enlarged section where the tapered waveguide is located, (c) cross-sectional view of the fabricated tapered waveguide cut along the major axis. Below insets are enlarged images of the inlet aperture and output aperture, respectively.

Because the designed plasmonic device has a 3-dimensional geometry, multiple masks with different sizes were loaded onto the used FIB machine. About 30 images are serially progressed with the decreasing order in size. In other words, the waveguide milling process proceeded with repetitive removal of thin disks. As a result, an elliptical tapered cone is formed at the center of the NSOM probe tip. After that, the bottom surface of the NSOM probe tip was polished until the output aperture has a 100 nm diameter in the minor axis direction at the end of the waveguide. Fig. 6 shows SEM images of the fabrication results. Fig. 6(a) shows the overall image of tapered waveguide structure embedded in a NSOM probe tip. As verified in Fig. 6(c), the desired waveguide shape was successfully achieved.

4. EXPERIMENTAL SETUP AND RESULTS

Fig. 7 shows a schematic diagram of the experimental setup which consists of a dispersion-compensation unit, noble gas chamber for HHG, and EUV detection unit. Since generated HHG signals are easily absorbed in the air, both the HHG part and EUV detection part should be placed inside a vacuum chamber in which pressure is maintained below 10^{-4} torr throughout experiment.

Dispersion of incident pulses was compensated. At the same time, the optical power and polarization of incident pulses were controlled by combining a half-wave plate and a linear polarizer. The used femtosecond laser provides a 10-fs pulse width, 75 MHz repetition rate, 800 nm center wavelength and 1.3 nJ per pulse from a titanium-sapphire oscillator. The original pulse width becomes broadened after passing through the half wave plate, linear polarizer, chamber window, focusing lens and air. If the pulse broadened in the time domain, the peak pulse power decreases even though the pulse energy remains the same. Therefore, as shown in Fig. 7, the temporal dispersion was compensated by use of multi-reflection between two chirped mirrors. Finally, the pulse width after the focusing lens was measured as 11 ~ 12 fs by the autocorrelation method.

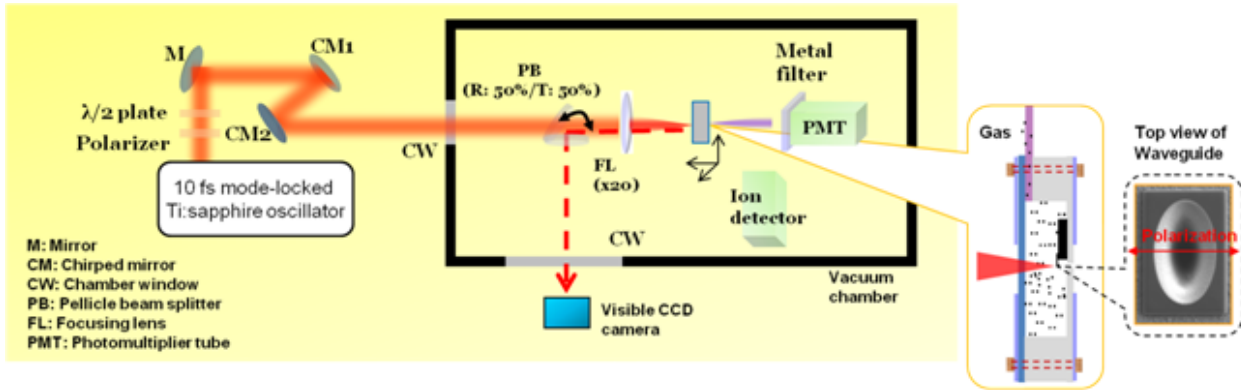


Fig. 7 Schematic diagram of experimental setup; the right inset shows the gas chamber and the tapered waveguide inside of it, M: mirror, CM: chirped mirror, CW: chamber window, PB: pellicle beam splitter, FL: focusing lens, PMT: photon multiplier tube. Note that laser polarization direction is parallel to the minor axis.

The delivered femtosecond laser is focused onto the inlet aperture of the tapered waveguide located inside the gas chamber. The average power of the incident laser pulses was set at 80 mW for HHG experiment, and the laser polarization direction is parallel to the minor axis of the ellipse cross-section. To precisely locate the laser focal spot onto the inlet aperture, a pellicle beam splitter was employed to monitor the relative position between the focusing lens and the waveguide structure. The reflected light from the upper surface of the tapered waveguide is guided toward the visible CCD camera installed outside the vacuum chamber for visual monitoring of alignment. After accurate beam alignment, the pellicle beam splitter is removed using a rotational stage. Also, noble gases such as Ar, and Xe are injected through a nozzle (diameter: 50 μm), thereby filling up the gas chamber within a short time. The gas pressure was controlled from 30 torr to 60 torr during HHG experiment.

The generated HHG signals in the EUV region are detected by a PMT (photomultiplier tube) with metal bandwidth filters. Previously, for the case of 2-D bow-tie array, a VLSG (varied-line spacing diffraction grating) was used to spectrally resolve the generated high harmonic signals. For the case of 3-D tapered waveguide structure, however, we used thin metal filters of narrow bandwidth in the EUV region. Since emitted EUVs from the tapered waveguide shows somewhat large divergence angles, the most of generated EUVs cannot reach the grazing incidence type spectrometer having a very narrow projection area at several hundreds of millimeters away. Metal filters have very various bandwidths and their transmittances depend on their constituent materials. For instance, a 250 nm-thick germanium (Ge) filter has 20 % transmittance for EUV wavelengths from 45 nm to 55 nm. Fig. 8 shows signal tendencies at both the ion detector and the PMT with a Ge filter.

Since the HHG process involves ionization of noble gas atoms, a large amount of ions is produced as well as high energy photons. For this reason, we could reconfirm the precise alignment of the incident laser beam onto the waveguide inlet aperture by observing the ion signal amplitude in the chamber using an ion detector located near the output side where high harmonic beams emit. As seen in Fig. 8(a), ionized atoms start to be monitored when the incident laser power is more than 50 mW. Since the maximal intensity enhancement is about on the order of 200 in the suggested waveguide structure, the incident laser power should be more than 50 mW in order to induce the multi-photon ionization required for HHG.

Both Fig. 8(b) and Fig. 8(c) shows the EUV signals detected by a PMT with a Ge filter. For both the cases, the incident laser power was 80 mW which is large enough and causes no thermal damage on the waveguide surface. We have verified the improved thermal robustness of the waveguide by checking with SEM, which reveals no sign of thermal deformation even after 10 hours of continuous operation.

Because the Ge filter allows light wavelengths between 45 nm and 55 nm to be transmitted with 20 % transmittance, only H15 (53 nm) and H17 (47 nm) signals can be detected with it. Fig. 8(b) and Fig. 8(c) show a significant difference in the detected signal amplitude vs. gas pressure, but the magnitude of the captured photon number remains similar. An intuitive physical explanation for the difference in the signal trend is still under investigation. The production rate of $10^7 \sim 10^8$ photons per second in this spectral range, i.e., H15 ~ H17, corresponds to the harmonic conversion efficiency of $10^{-8} \sim 10^{-9}$ when taking into account filter transmittance.

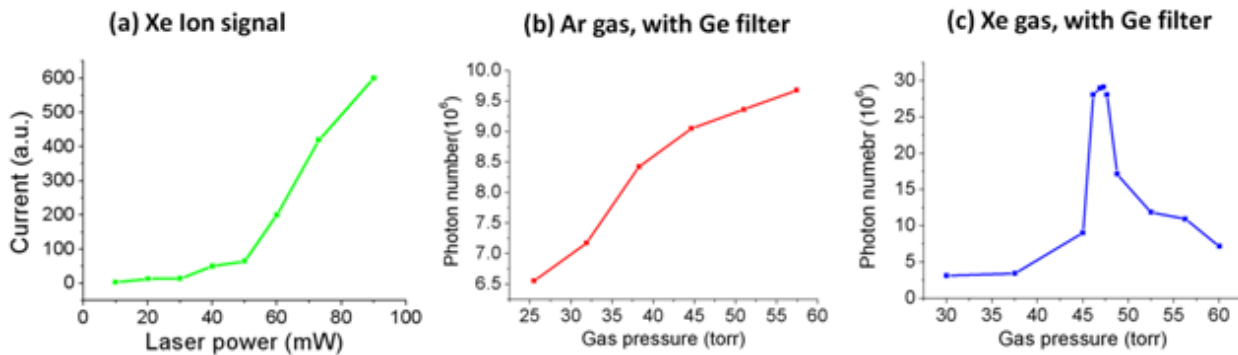


Fig. 8 Detected HHG signals at (a) the ion detector with Xe gas and pressure at 47 torr. (b) by the PMT with Ge filter from Ar gas, and (c) the PMT with Ge filter for Xe gas; both for (b) and (c), the incident laser power is 80 mW.

Also, It can be reversely calculated how much the laser field is amplified by manipulating the HHG cutoff formula of

$$E_{\text{cut-off}} = I_p + 3.17U_p \quad (1)$$

where E_{max} is the maximum energy of harmonic photon, I_p is the ionization energy of the target gas, U_p is the ponderomotive potential. For a linearly polarized oscillating field, U_p [eV] has a form of

$$U_p = 9.33 \times 10^{-14} I_L \lambda^2 \quad (2)$$

where I_L [Wcm^{-2}] is the intensity, λ [μm] is the wavelength of the incident femtosecond laser. From the generated harmonic signals detected by the PMT with noble gas injection, E_{max} can be set to 26.4 eV at least, because the maximum harmonics possibly detected in our experimental system is the 17th order. By adopting the 1st ionization energy of Ar (15.8 eV) and Xe (12.1 eV), the enhanced laser intensity of the femtosecond laser was calculated as $5.6 \times 10^{13} \text{ Wcm}^{-2}$ and $7.6 \times 10^{13} \text{ Wcm}^{-2}$, respectively. Therefore, if we assume that incident laser has an initial intensity of $4.6 \times 10^{11} \text{ Wcm}^{-2}$ and the focal spot size is 5 μm (FWHM), it was experimentally verified that the peak intensity of the initial laser pulse is amplified at least by more than a factor of 20 dB. These estimations are in accordance with the numerical prediction by FDTD analysis.

5. CONCLUSIONS

We investigated HHG based on guided SPPs accumulated at the output side of a tapered hollow waveguide structure. As in the 2-D bow-tie nanoantenna structure, the peak intensity of an incident pulse laser can be largely enhanced by excited SPPs propagating along the tapered surface of the MDM or DMD waveguide structure. By optimizing the MDM tapered waveguide parameters by FDTD simulation, the 20-dB volume where the field enhancement factor becomes more than 20 dB can be expanded about a thousand times than that of a single bow-tie antenna. The optimized tapered waveguide has an elliptical cross-section and the size of the output aperture where generated HHG signals radiate is far less than the fundamental wavelength. From HHG experiment, it was experimentally verified that the incident pulse intensity is amplified by a factor of more than 20 dB at least, thereby producing high harmonics successfully. We detected high harmonic signals up to 17th order by using a PMT with thin metal filters whose transmission range lies in the EUV spectral region. Therefore, the designed plasmonic waveguide structure can play a role of not only coherent EUV pulse generator but also nano-lasing source emitted from a sub-wavelength-scale aperture. Since the suggested plasmonic structure can be fabricated onto a commercial NSOM probe, this compact, coherent EUV light source can be incorporated with various applications of near-field optics such as Raman spectroscopy, microscopy, lithography and surface metrology.

ACKNOWLEDGMENT

This work was supported by the Creative Research Initiative Program of the Ministry of Science and Technology of the Republic of Korea.

REFERENCES

- [1] Barnes, W. L., Dereux, A., and Ebbesen, T. W., "Surface plasmon subwavelength optics," *Nature*, 424, 824-830 (2003).
- [2] Campion, A., and Kambhampati, K., "Surface-enhanced Raman scattering," *Chemical Society Reviews*, 27, 241-250 (1998).
- [3] Kneipp, K., Wang, Y., Kneipp, H., Perelman, L. T., Itzkan, I., Dasari, R.R., and Feld, M. S., "Single molecule detection using surface-enhanced Raman scattering (SERS)," *Phys. Rev. Lett.* 78, 1667-1670 (1997).
- [4] Nie, S., and Emory, S. R., "Probing Single Molecules and Single Nanoparticles by Surface-Enhanced Raman Scattering," *Science*, 275, 1102-1106 (1997).
- [5] Hecht, B., Sick, B., Wild, U. P., Deckert, V., Zenobi, R., Martin, O. J. F., and Pohl, D.W., "Scanning near-field optical microscopy with aperture probes: Fundamentals and applications," *J. Chem. Phys.*, 112, 7761 (2000).
- [6] Volkov, V. S., Bozhevolnyi, S. I., Devaux, E., Laluet, J. Y., and Ebbesen, T. W., "Wavelength Selective Nanophotonic Components Utilizing Channel Plasmon Polaritons," *Nano Lett.*, 7, 880-884 (2007).
- [7] Ropers, C., Neacsu, C. C., Elsaesser, T., Albrecht, M., Raschke, M. B., and Lienau, C., "Grating-Coupling of Surface Plasmons onto Metallic Tips: A Nanoconfined Light Source," *Nano Lett.*, 7, 2784-2788 (2007).
- [8] Mühlischlegel, P., Eisler, H. J., Martin, O. J. F., Hecht, B. and Pohl, D. W., "Resonant optical antennas," *Science*, 308, 1607-1609 (2005).
- [9] Jin, E. X., Xu, X., "Enhanced optical near field from a bowtie aperture," *Appl. Phys. Lett.* 88, 153110 (2006).
- [10] Pedaci, F., Wang, Y., Berrill, M., Luther, B., Granados, E. and Rocca, J.J., "Phase-coherent, injection-seeded, tabletop soft-X-ray lasers at 18.9 nm and 13.9 nm," *Nature Photonics*, 2, 94-98 (2008).
- [11] Corkum, P. B., "Plasma perspective on strong field multiphoton ionization," *Phys. Rev. Lett.*, 71, 1994-1997 (1993).
- [12] Strickland, D., Mourou, G., "Compression of amplified chirped optical pulses," *Opt. Comm.* 56, 219-221 (1985).
- [13] Gohle, C., Udem, T., Herrmann, M., Rauschenberger, J., Holzwarth, R., Schuessler, H. A., Krausz, F. and Hänsch, T. W., "A frequency comb in the extreme ultraviolet," *Nature*, 436, 234-237 (2005).
- [14] Kim, S., Jin, J., Kim, Y. J., Park, I. Y., Kim, Y. and Kim, S. W., "High-harmonic generation by resonant plasmon field enhancement," *Nature*, 453, 757-760 (2008).
- [15] Stockman, M. I., "Nanofocusing of optical energy in tapered plasmonic waveguides," *Phys. Rev. Lett.*, 93, 137404 (2004).

- [16] Zia, R., Selker, M. D., Catrysse, P. B., and Brongersma, M. L., "Geometries and materials for subwavelength surface plasmon modes," *J. Opt. Soc. Am. A*, 21, 2442-2446 (2004).
- [17] Ayars, E. J., and Hallen, H. D., "Surface enhancement in near-field Raman spectroscopy," *Appl. Phys. Lett.*, 76, 3911 (2000).
- [18] Liu, Z., Steele, J. M., Srituravanich, W., Pikus, Y., Sun, C., and Zhang, X., "Focusing Surface Plasmons with a Plasmonic Lens," *Nano Lett.*, 5, 1726-1729 (2005).
- [19] Lin, Y., Hong, M. H., Wang, W. J., Law, Y. Z., and Chong, T. C., "Sub-30 nm lithography with near-field scanning optical microscope combined with femtosecond laser," *Appl. Phys. A* 80, 461-465 (2005).
- [20] Bouhelier, A., "Field-enhanced scanning near-field optical microscopy," *Microsc. Res. Tech.* 69, 563-579 (2006).
- [21] Fromm, D.P., Sundaramurthy, A., Schuck, P.J., Kino, G. and Moerner, W. E., "Gap-dependent optical coupling of single "bowtie" nanoantennas resonant in the visible," *Nano Lett.* 4, 957-961 (2004).
- [22] Grober, R. D., Schoelkopf, R. J. and Prober, D. E., "Optical antenna: Towards a unity efficiency near-field optical probe," *Appl. Phys. Lett.* 70, 1354-1356 (1997).
- [23] Nisoli, M., "Nanoplasmonics: Brave new attoworld," *Nature Photonics*, 1, 499-500 (2007).
- [24] Dionne, J. A., Sweatlock, L. A., and Atwater, H. A., "Planar metal plasmon waveguides: frequency-dependent dispersion, propagation, localization, and loss beyond the free electron model," *Phys. Rev. B.*, 72, 075405 (2005).
- [25] Choi, H., Pile, D. F., Nam, S., Bartal, G., and Zhang, X., "Compressing surface plasmons for nano-scale optical focusing," *Optics Express*, 17, 7519-7524 (2009).
- [26] Novotny L., and Hafner, C., "Light propagation in a cylindrical waveguide with a complex, metallic, dielectric function," *Phys. Rev. E.*, 50, 4094-4106 (1994).
- [27] The Nascatech GmbH company (Germany), <http://www.nascatech.com/>